Model-based signal processing enables bidirectional inferring between local field potential and spikes evoked by noxious stimulation

François Gabrielli, M. Megemont, R. Dallel, P. Luccarini, L. Monconduit

Version of Record: https://www.sciencedirect.com/science/article/pii/S0361923021001647
Manuscript_8d12867a6738a5ca3e557c56be9ec098

Model-based signal processing highlights bidirectional inferring between pain-evoked local field potential and spikes

Gabrielli F.[1], Megemont M.[1,2], Dallel R.[1], Luccarini P.[1], Monconduit L.[1]

[1] Université Clermont Auvergne, CHU Clermont-Ferrand, Inserm, Neuro-Dol, F-63000 Clermont-Ferrand, France

[2]Department of Molecular, Cell and Systems Biology, University of California, Riverside, CA 92521, USA

Abstract

Background: Chronic pain is associated with abnormal levels of electrical excitability of the somatosensory cortex neurons. Consequently, recording spontaneous and evoked activities by means of unitary extracellular recordings and local field potential (LFP) are key understanding the mechanisms behind such alterations. There is a growing need to highlight the relationship between spiking activity and LFP. Here, we hypothesized that LFP could be inferred from spikes under evoked conditions.

Method: We detail a process to highlight the C-fiber (pain) evoked activity, by removing the A-fiber evoked activity using a model-based approach. Then, we applied the convolution kernel theory and optimization algorithms to infer the C-fiber LFP from the single cell spikes. Finally, we used a probability density function and an optimization algorithm to infer the spikes distribution from the LFP.

Results: We successfully extracted C-fiber LFP in all data recordings. We observed that C-fibers spikes preceded the C-fiber LFP and were rather correlated to the LFP derivative. Finally, we inferred LFP from spikes with excellent correlation coefficient (r = 0.9) and reverse generated the spikes distribution from LFP with good correlation coefficients (r = 0.7) on spikes number.

Conclusion: We introduced the kernel convolution theory to successfully infer the LFP from spikes, and we demonstrated that we could reverse generate the PSTH from the LFP.

Keywords
Pain, evoked, local field potential, single cell electrophysiology, signal processing, convolution, ergodicity

Highlights

- Evoked spikes preceded the depression in Local Field Potential
- Evoked LFP is the result of spikes convoluted by a kernel
- Evoked PSTH can be inferred from LFP using a probability density function of spikes

1. Introduction

Understanding how information is encoded in neural systems requires monitoring a substantial fraction of the neuronal population (Georgopoulos et al., 1986). The local field potential (LFP) is one of the most popular and easy methods to measure the population activity. Unfortunately, LFP is also known to be difficult to interpret and model (Buzsáki et al., 2012; Einevoll et al., 2013). These difficulties stem from the fact that LFP is a composite signal of synaptic currents and spiking patterns of multiple neurons (Buzsáki et al., 2012). Thus, highlighting the relationship between spiking activity and LFP is a major issue that requires an improvement to existing analysis methodologies of electrophysiological signals. The most common approach to analyze the spikes/LFP relationship consists of averaging the LFP on a small window around each spike time to get the Spike Time Average (STA) (Denker et al., 2011; Geng et al., 2019; Nauhaus et al., 2009; Ray, 2015; Ray and Maunsell, 2011). The STA is then processed with the spike train, usually through a convolution, to reconstruct the theoretical LFP and compared to the measured LFP. Additional methods such as maximum likehood (Cui et al., 2016), Hammerstein-Wiener model (Bai et al., 2014), L1 sparse approach (Bighamian et al., 2019), Volterra mode (Zanos et al., 2011), MIMO model (Hall et al., 2014), Generalized Linear model (Arai and Kass, 2017) or Markov chains (Galindo-Leon and Liu, 2010) were also proposed to describe the spikes/LFP relationship. Most of these studies were interested in LFP during spontaneous activity, in which convergent neurons respond to asynchronous signals coming from very heterogenous inputs. Moreover, since LFP is considered as a local, grouped activity (Lindén et al., 2011; Liu et al., 2015), its spontaneous fluctuations are subject to the activity of different nearby neurons. Thus, although spontaneous recordings are closer to normal neural activity, the resulting system is complex to analyze, and even very innovative methods achieved medium results. Because previously stated (Denker et al., 2011) spikes/LFP relationship could only be highlighted when a group of neurons fires synchronously (Storchi et al., 2012; Zippo et al., 2014), we investigated the spikes/LFP relationship in evoked conditions to reduce the number of inputs and synchronize the activity of neurons.

We hypothesized that in evoked conditions, the most important contribution to the LFP is the spike pattern. To test this hypothesis, we studied the spikes/LFP relationship in the medullary dorsal horn (MDH) that receives nociceptive inputs from the head and neck. Based on electrophysiological recordings of MDH neuron response to facial electrical stimulation of nociceptive C-fibers, we first assessed whether LFP and spikes are synchronized. Then we aimed to reconstruct LFP from the evoked spike pattern, using a model-based approach based on convolution kernel theory (Nawrot et al., 1999; Shimazaki and Shinomoto, 2010). Finally, we tested whether the spike pattern could be reconstructed from the LFP.

2. Materials and methods

2.1. Animals

Adult male Sprague-Dawley rats (250–300 g; Charles River, L'Arbresle, France) were stabulated at 23 ± 1 °C in plastic cages (425 x 266 x 185 mm , 2-3 rats per cage; Tecniplast, Comerio, Italy) with soft bedding and water and food ad libitum in a 12-h/12-h dark/light cycle for at least one week before experiment.

Animal experiments were performed according to the ethical guidelines of the International Association for the Study of Pain, the Directive 2010/63/UE of the European Parliament and the Council on the protection of animals used for scientific purpose. Protocols for animal care and use applied in this work were approved by the appropriate local committee at the University of Clermont-Ferrand-Auvergne and authorized by The Research Ministry (nb #7080, #12899, # 18346). All experiments, analysis, and reports followed the ARRIVE guidelines, and were carried out in accordance with the U.K. Animals (Scientific Procedures) Act, 1986 and associated guidelines, EU Directive 2010/63/EU for animal experiments, or the National Institutes of Health guide for the care and use of Laboratory animals (NIH Publications No. 8023, revised 1978). All efforts were made to minimize the number of animals used.

The protocols used for the animal surgery were like those described previously (Boyer et al, 2014; Flores Ramos et al., 2017). Briefly in vivo electrophysiological recordings within the MDH were performed under 2% isoflurane (Aerane®, Baxter SAS) in a NO2/O2 mixture (1/3 – 2/3). After tracheal cannulation to perform artificially ventilation, carotid artery and external jugular vein catheterized, animals were paralyzed by an i.v. perfusion of vecuronium bromide (2.4 mg/h). The level of isoflurane, O2, N2O and the end-tidal CO2 (3.5–4.5%) were monitored during the entire experimental period by a gaz monitoring system (Dragër®, Vamos, Allemagne). Colorectal temperature was kept at 37 ± 0.5 °C. The animals were placed in a stereotaxic frame with the head fixed in a ventroflexed position. The trigeminocervical complex was exposed by removing the overlying musculature, atlanto-occipital membrane, dura mater and a cervical laminectomy. The dura overlying the dorsal surface of the right hemisphere and transverse sinus was exposed and flooded with artificial cerebro-spinal fluid. After surgery, the level of isoflurane was reduced to 0.75% and maintained at this level during the recording period.

2.2. Electrophysiological recording and electrical stimulation

Unitary extracellular recordings Glass microelectrodes (2-8 MΩ) filled with 5% NaCl containing pontamine sky blue were used to record activities within the right MDH. The electrophysiological setup was essentially as described previously (Boyer et al., 2014; Flores Ramos et al., 2017). Briefly, on a first channel, single-unit activities were amplified on a differential amplifier (50 Hz band-stop filter, High pass filter 10 KHz, low pass filter 300 Hz, gain 103). The activities recorded went into a window discriminator (WPI, 121 Windows discriminator) connected to a CED 1401plus interface (Cambridge Electronic Design) and a PC computer (Spike 2® version 6.16 software, CED, Cambridge, UK). On a second channel, the LFP and spikes were recorded with the same microelectrode, amplified (No band-stop filter, High pass filter 0.1 Hz, low pass filter 10k Hz, gain 10^2) and directly connected to a PC through CED 1401plus interface.
A systematic search for MDH neurons responding to percutaneous electrical stimuli was performed. Electrical square-wave stimuli (2 ms duration, 2-8mA intensity) were applied through a pair of stainless-steel needle electrodes subcutaneously placed on the face to elicit two peaks of activation at different but fixed latencies. According to literature (Burgess and Perl, 1973; Gasser and Erlanger, 1927), these two peaks correspond to peripheral conduction velocities in the A- and C-fiber ranges, respectively.
A total of 18 animals underwent the following procedure. Once a MDH neuron was identified, we applied multiple series of 30 cutaneous electrical stimulations, from 6 to 19 depending on the duration of the recording, for a total of 232 series. Stimulation period was 1500ms and series period was 15 min. Data were analyzed using post-stimulus time histograms (PSTH).

2.3. Signal preprocessing

The electrophysiological responses recorded by the CED software were stored in a binary file for data analysis and processing using homebrew Matlab code (© 2014 The MathWorks, Inc.). Recordings

were synchronized with the electrical stimulation, denoised from 50Hz artifact, and spikes were removed using a 3rd order, 31 points Savitzky-Golay filter (Savitzky and Golay, 1964), as presented figure 1.

2.4. C-fiber evoked LFP extraction algorithm

Signals were then smoothed by calculating the median value over 30 stimulations. The analysis will now focus on the C-fiber LFP. In order to remove the A-fiber LFP from the signal, the first step was to identify the A-fiber LFP, which was modelled as a single exponential curve. To this end, segments of signal were selected manually with four time stamps placed (figure 2): one at the max depression of the A-fiber LFP (t_1), one at the beginning of the C-fiber LFP usual timing (t_2), one at the end of the C-fiber LFP (t_3), and one at the end of LFP recording (t_4).

The (t_1-t_2) and (t_3-t_4) portions of the LFP only are used as the curve to match for the algorithm. Then, a non-linear least-squares approach (Newton-Gauss) was used to model the A-fiber LFP depression. Finally the modelled A-fiber LFP was removed to extract only the C-fiber LFP (Björck, 1996). See above for iterative steps, with the following model and Jacobian matrix:

$$s(t) = LFP_C(t) + \sigma(t) + K_0 e^{-\frac{t}{\tau}} + K_1 + a.t$$

$$\boldsymbol{J} = \begin{bmatrix} \frac{\partial s}{\partial K_0} \\ \frac{\partial s}{\partial \tau} \\ \frac{\partial s}{\partial K_1} \\ \frac{\partial s}{\partial a} \end{bmatrix} = \begin{bmatrix} e^{-\frac{t}{\tau}} \\ \frac{K}{\tau^2} e^{-\frac{t}{\tau}} \\ 1 \quad \dots \quad 1 \\ t \end{bmatrix}$$

With s being the total LFP, LFP_C the C-fiber LFP, σ a random noise, K_0 the amplitude of the A-fiber LFP model, τ the decay rate of the A-fiber LFP model, K_1 the offset, and a the linear drift. Stop criterion was the same as above. Once the algorithm had converged, the A-fiber LFP model was subtracted from the LFP to extract the C-fiber LFP depression (see figure 7.A and 7.B for result).

2.5. Analysis of LFP – spikes synchronization

To characterize the synchronization between the spikes and LFP, we analyzed the C-fiber portion of the PSTH by using only the spiking time within 50ms-150ms. We then transformed the PSTH into a continuous variable using the averaged sliding windows to produce a smoothed PSTH. We also calculated the time derivative of the LFP and analyzed the time relationship between smoothed PSTH and LFP by comparing the latencies between the peaks of each signal.

Also, we considered the PSTH as a reflection of the underlying firing frequency. That observation led us to consider applying the kernel convolution to explain the relationship between spikes and LFP.

Briefly, spike latencies corresponding to the 30 stimulations used to calculate the LFP were gathered to provide a binary spiking variable: a continuous vector of '0' (no spike) and '1' (spike) at the same sampling frequency than the LFP. That binary variable was then convoluted with a kernel, smoothed using a Savitzky-Golay filter, and compared to the LFP. The kernel's parameters that produced the best fit was a double exponential decay:

$$kernel\ \ (K_1, \tau_1, \tau_2, t_0, K_2, t) = K_1 e^{-\frac{(t-t_0)}{\tau_1}} . \left(1 - e^{-\frac{(t-t_0)}{\tau_2}}\right) + K_2$$

With K_1 the amplitude (µV),τ_1 the decay rate (in ms), τ_2 the rising rate (in ms), t_0 a minor delay (usually less than 1ms) representing a spike-to-LFP propagation time, and K_2 the offset correction.

In order to find the best parameters, we needed a cost function to minimize. Let f be the function that takes the spikes binary information as vectoral input (***spikes***), and returns the LFP as output:

$$LFP = f\ \ (K_1, \tau_1, \tau_2, t_0, K_2) = SG\big(\boldsymbol{spikes} * kernel\ \ (K_1, \tau_1, \tau_2, t_0, K_2, \boldsymbol{T})\big)$$

With (*) operator being the convolution, SG is a Savitzky-Golay filter of 2nd order and window length of 5ms, and $\boldsymbol{T}$ the time vector corresponding to the recorded LFP. Let $\boldsymbol{\lambda}$ be the vector of parameters: $\boldsymbol{\lambda} = [K_1, \tau_1, \tau_2, t_0, K_2]$. We used the SIMPLEX algorithm(Lagarias et al., 1998) to find the optimal parameters $\boldsymbol{\lambda_{opti}}$ that minimize the Euclidian norm of the difference between f and measured LFP, to demonstrate that we could find a kernel that transforms the spike pattern into LFP. See figure 3 for an illustration of the convolution process.

$$\begin{cases} LFP\_calculated = f(\boldsymbol{\lambda_{opti}}) \\ with \\ \boldsymbol{\lambda_{opti}} = \min_{\boldsymbol{\lambda}} \|LFP_C - f(\boldsymbol{\lambda})\| \end{cases}$$

Method performance was assessed using Pearson correlation coefficient between measured LFP and calculated LFP from convolution.

To prove the previous approach can be reversed and that the spiking activity or PSTH can be accurately produced from the LFP, we introduce an approach based on the probability density function (PDF): this approach is not used to produce spikes, but a distribution of spikes. We randomly generate a volley of spikes that follow the PDF, calculate the LFP using convolution method, and compare that calculated LFP to the measured LFP. The method consists of finding the best parameters of the PDF and the best spikes number that minimize the difference between measured LFP and calculated LFP. We finally output the spikes timing and the PSTH.

We used the legit function (inverse of logistic function) to produce the spike sequence (L) of N spikes, with a mean value μ and a spread value σ, and a probability $x \in [0,1]$:

$$L_{\mu,\sigma}(x) = \mu + \sigma . ln\left(\frac{x}{1-x}\right)$$

The variable x was linearly spaced from 0 to 1, over N values, to build a vector of size N, $\boldsymbol{X}_N$.

The L function was then transformed into a three variables function:

$$L(\mu, \sigma, N) = \mu + \sigma . ln\left(\frac{\boldsymbol{X}_N}{1-\boldsymbol{X}_N}\right)$$

Such L function produces a probability distribution function, similar to a gaussian function, equals to :

$$\mathrm{PDF}_{\mu,\sigma}(X) = \frac{e^{-\frac{X-\mu}{\sigma}}}{\left(1+e^{-\frac{X-\mu}{\sigma}}\right)^2}$$

The global PDF that was used in the present paper was combinations of two PDF. As a result, the final function that produces the spiking probability is:

$$L(\mu_{1,2}, \sigma_{1,2}, N_{1,2}) = L(\boldsymbol{\mu}, \boldsymbol{\sigma}, \mathbf{N}) = \sum_{i=1}^{2} \mu_{\mathrm{i}} + \sigma_i . ln\left(\frac{\boldsymbol{X}_{N_i}}{1-\boldsymbol{X}_{N_i}}\right)$$

With μ_i being the mean values of the i[th] distribution, σ_i the spread of the i[th] distribution, and N_i the number of spikes of the i[th] distribution. The L function can produce a distribution of spikes of different shapes. From that sequence of spikes, we calculated the PSTH and calculated the LFP again by convoluting the kernel, using the following equation:

$$LFP_{calculated} = g(\boldsymbol{\mu}, \boldsymbol{\sigma}, \mathbf{N}) = SG(L(\boldsymbol{\mu}, \boldsymbol{\sigma}, \mathbf{N}) * kernel)$$

With (*) operator being the convolution and SG is a Savitzky-Golay filter of 2[nd] order and window length of 5ms. The SIMPLEX algorithm was used to find the optimal parameters $(\boldsymbol{\mu}, \boldsymbol{\sigma}, \mathbf{N})$ that minimized the Euclidian error between the measured LFP and the computed LFP.Overall we reconstructed the PSTH by calculating the optimal spike distribution that, once convoluted with the corresponding kernel, fitted with measured LFP.

$$\begin{cases} PSTH = histogram(L(\boldsymbol{\mu_{opti}}, \boldsymbol{\sigma_{opti}}, \mathbf{N_{opti}})) \\ and \\ LFP_{reconstructed} = g(\boldsymbol{\mu_{opti}}, \boldsymbol{\sigma_{opti}}, \mathbf{N_{opti}}) \\ with \\ \boldsymbol{\mu_{opti}}, \boldsymbol{\sigma_{opti}}, \mathbf{N_{opti}} = \underset{\boldsymbol{\mu},\boldsymbol{\sigma},\boldsymbol{N}}{\operatorname{argmin}} \left\| LFP_{C\_measured} - g(\boldsymbol{\mu}, \boldsymbol{\sigma}, \mathbf{N}) \right\| \end{cases}$$

As an example, with the same number of spikes, the proposed method can reproduce different PSTH width and maximum by changing the mean values (figure 4.A and 4.C). It can also generate a double peak shape, either with similar maximum and width (figure 4.D), or a more complex shape with a narrow peak followed by a smaller and wider peak (figure 4.B), such as the typical C-fiber evoked activity with highly synchronized early spikes and diffused late spikes.

2.6. Statistical analysis

The method performance was assessed using Pearson correlation coefficient and regression coefficient between measured number of spikes and calculated number of spikes. Statistical analyses were done by first testing the normality of distributions with a LillieFors (Lilliefors, 1967) test, and depending on the result, a two-sample or paired t-test or a Wilcoxon rank-sum test. All tests were done with Matlab Statistical Toolbox (© 2014 The MathWorks, Inc.).

3. Results

3.1. Extraction of C-fiber evoked activity in LFP

After denoising the data signal and separating LFP from spikes, we successfully extracted C-fiber LFP in all the data recordings, even when the C-fiber LFP was much smaller than the A-fiber LFP (figure 5). Thus, this result demonstrates the efficiency of the process and its ability to extract all C-fiber LFP (figure 5), even within short latency with the A-fiber LFP. Overall, 90% of C-fiber LFP did not exceed 40% of A-fiber LFP amplitude, with a most common ratio at about 10%.

3.2. LFP - spikes relationship

3.2.1. LFP – spikes synchronization

We observed that the maximum rate of the PSTH, around 70-80ms, preceded the maximum depression of C-fiber LFP, around 100ms. Those observations suggest that the C-fiber spikes were anterior to C-fiber LFP based on our measurements. We, therefore, compared the PSTH to the variation rate of the LFP, brought by the time derivative (figure 6). Our results showed PSTH latencies, including the double peaks of the C-fiber evoked activity, fit the derivative of the LFP, and not the LFP itself (figure 6A). In order to confirm that observation, the latency from the peak value of PSTH to peak value of LFP, and the latency from peak value of PSTH to peak value of the derivative of LFP were calculated and compared (figure 6B). Our results showed that absolute latencies between maximum depression of PSTH and maximum depression of derivative of C-fiber LFP were lower than absolute latencies between peak of PSTH and maximum depression of C-fiber LFP.

3.2.2. Reconstruction of LFP from spikes

The existence of a relationship between PSTH and C-fiber LFP derivative confirms that spike pattern is a significant component of LFP. Consequently, C-fiber LFP should be reconstructed from spikes. To test this hypothesis, we successfully convoluted spike trains with a kernel characterized by a double exponential decay. Though the kernel convolution did not allow the reconstruction of all the subtle variations of the recorded C-fiber LFP, our method successfully reconstructed the main LFP dynamic (figure 7). In order to assess the efficiency of the approach, measured and calculated LFP were linearly correlated using Pearson correlation coefficient.

The average correlation coefficient r^2 between the recorded and calculated C-fiber LFP was 0.90. Thus, our results validated that LFP can be inferred from spikes through kernel convolution.

3.2.3. Reconstruction of PSTH from LFP

The next step was to assess whether the PSTH can be calculated from the LFP. We used the method of PDF that allowed us to model spike probability, generate the LFP with the kernel convolution, and compare it to the measured LFP. Calculated PSTH were very close to the actual measured PSTH (figure 8), with peak timing of PSTH and global shape very comparable.

Final performance of the calculation of PSTH from the LFP was assessed by correlating the total number of spikes from calculation and measurement, and overall goodness-of-fit was assessed using Pearson coefficient on total spikes number. Correlation was done in two folds: the method was good if correlation coefficients were close to 1 (same variation), and if regression coefficients were also close to 1 (spike numbers were the same).

Overall, calculated spike number was highly correlated to actual measured spike number for the C-fiber evoked activity (figure 8.B): the correlation coefficient was 0.8, and regression coefficients was 0.7. The proposed distribution led to an underestimation of the spike number by 30%.

4. Discussion

We described a method to analyze the relationship between C-fibers evoked spikes and LFP in low signal-to-noise ratio of unitary extracellular recordings. Our results showed that it is possible to assess the relationship between LFP and spikes pattern, in both ways, although some studies predicted otherwise (Herreras, 2016), mainly thanks to the evoked condition and the proposed methods.

Concerning the relationship between spikes, LFP and time derivative of the LFP, our results confirm similar conclusions in previously published studies (Storchi et al., 2012; Zippo et al., 2014). Namely, PSTH variations correspond to the variations of the first derivative of LFP and not to the variation of the LFP itself. In addition, spikes volley precedes LFP depression, confirming previous observations, visible on facial pain-evoked recording of LFP (Melin et al., 2017) or sound-evoked recording in auditory cortex (Liu et al., 2015). Therefore, LFP depression may not be the image of presynaptic events, as the resulting depression would appear before the peak of PSTH. One suggestion can be that presynaptic events generate spikes with a well-known mechanism, and also generate the LFP depression, but with a separate delay and mechanism. As a result, such a construction would build a model with one input (presynaptic events) and two outputs (spikes and LFP).
This suggests a causality link from spiking activity to LFP variation rate and not with the LFP raw itself. As a consequence, this result may be in conflict with the studies that correlate spike with LFP such as the spike triggered LFP or the spike-LFP phase (Einevoll et al., 2013; Vinck et al., 2012) , or the link between spiking frequency and LFP state (Kelly et al., 2010). The main difference comes from the experimental context. Those studies were based on spontaneous activity whereas our work was based on evoked conditions where the neurons receive similar and synchronized inputs. This generates a deeper LFP signature, synchronized with spiking activity. This observation is in accordance with previous studies (Denker et al., 2011) which concluded that spikes synchronization is a key factor to explaining LFP oscillations.

Recent works have investigated the relationship between spiking activity and LFP, and worked on generation of firing frequency from LFP, based on Support vector Machine (Rasch et al., 2008) or least squared correlation (Hall et al., 2014). Best correlation coefficients obtained through their proposed method were respectively 0.4 and 0.52 on firing rate. Our approach revealed to be more efficient and reached a correlation coefficient of $r = 0.77$ on spikes number. Again, such improvement can be explained by the evoked conditions compared to spontaneous activity. In this last condition, LFP reflects mainly the network activity, and is probably polluted by the diversity of inputs.
Overall, the ability to recover the PSTH from the LFP only is a huge improvement for extracellular recording. Indeed as LFP is easier to record than single cell activity (Maling and McIntyre, 2016), we could estimate the neuronal activity from the LFP. However, our method also comes with some limitations. We proved that LFP could be inferred from spikes through a convolution process, but the very same kernel was needed to infer the PSTH from the LFP. Consequently, inferring the PSTH from the LFP in our experimental conditions would not be currently possible without previously identifying

the convolution kernel. Additional work is needed to generalize the convolution kernel or at least provide a minimal set of functions instead of a mathematical model to be fitted.

The possibility to rebuild spike activity from LFP also provides information about the organization of MDH network. LFP is often considered as a spatial integration of the neuronal activity (Herreras, 2016; Lindén et al., 2011). So, if we see the signature of a stimulation in the LFP, such as the C-fiber evoked activity due to the electrical stimulation of C-fiber, the surrounding neurons must be involved in processing the same stimulation. Thus, being able to calculate the PSTH from LFP or LFP from PSTH suggests that evoked neuronal activity in MDH can be seen as an ergodic system (Pardalos and Principe, 2002; von Plato, 1991). In such a system, repeated stimulations of one neuron lead to the same statistical response as a single stimulation of a population of neurons. Therefore, and due to the somatotopic organization of the MDH, ergodicity may be a signature of both spatial organization of neurons and their synchronization.
Now, it is well known that during single cell recording, the simultaneously recorded LFP comes from surrounding neurons, up to 200 µm (Lindén et al., 2011), and this property induces limitations to our work. Assuming the ergodicity in MDH, we used only a single convolution function for one recording, but we cannot be sure all neurons generating the LFP would follow the same convolution function. Therefore, our approach did not achieve perfect reconstruction, and future work will try to include multiple convolutional functions in order to reflect the participation of all neurons to the LFP.
In addition, our method underestimates the total spikes number, by about 30%, whereas the corresponding LFP was correctly reconstructed. This was assumed to come from the smoothing step of the LFP. Indeed, the Savitsky-Golay filter eliminates all fast-changing elements from the signal, and sparse spikes were deleted in the process. As a result, the process produced the good fitting LFP with less spikes.
Secondly, we used a single electrode to record single cell activity and LFP. As previously stated in literature (Herreras, 2016), we need multiple electrodes to better understand the relationship between single cell activity and LFP. This would lead to proper source separation to associate separate convolution function to each neuron. Moreover, this would allow us to understand the small fluctuation in the LFP that are not generated by the evoked conditions, such as during spontaneous recording.

5. Conclusion

We hypothesized that a reciprocal relationship exists between single cell extracellular recording and LFP under evoked conditions in the MDH. We successfully demonstrated that PSTH were correlated to time derivative of LFP instead of raw LFP. In addition, we introduced the kernel convolution theory to successfully infer the LFP from spikes, and we demonstrated that, despite some limitations, we could reverse generate the PSTH from the LFP. Those results bring a new insight on how spikes and local field potential are connected in evoked conditions.

Author contribution statement

François Gabrielli: Conceptualization, Methodology, Data Curation, Formal analysis, Software, Writing - Original draft. **Marine Megemont**: Investigation, Conceptualization, Writing- Original draft, Visualization. **Philippe Luccarini**: Investigation. **Radhouane Dallel**: Resources. **Lénaïc Monconduit**: Writing- Reviewing and Editing, Supervision.

Acknowledgments

The authors thank Jennifer Shyong for providing language help.

References

Arai, K., Kass, R.E., 2017. Inferring oscillatory modulation in neural spike trains. PLoS Comput. Biol. 13, e1005596. https://doi.org/10.1371/journal.pcbi.1005596

Bai, W., Yi, H., Liu, T., Wei, J., Tian, X., 2014. Incoordination between spikes and LFPs in Aβ1−42-mediated memory deficits in rats. Front. Behav. Neurosci. 8. https://doi.org/10.3389/fnbeh.2014.00411

Bighamian, R., Wong, Y.T., Pesaran, B., Shanechi, M.M., 2019. Sparse model-based estimation of functional dependence in high-dimensional field and spike multiscale networks. J. Neural Eng. 16, 056022. https://doi.org/10.1088/1741-2552/ab225b

Björck, Åke., 1996. Numerical Methods for Least Squares Problems, Other Titles in Applied Mathematics. Society for Industrial and Applied Mathematics. https://doi.org/10.1137/1.9781611971484

Boyer, N., Dallel, R., Artola, A., Monconduit, L., 2014. General trigeminospinal central sensitization and impaired descending pain inhibitory controls contribute to migraine progression. Pain 155, 1196–1205. https://doi.org/10.1016/j.pain.2014.03.001

Burgess, P.R., Perl, E.R., 1973. Cutaneous Mechanoreceptors and Nociceptors, in: Albe-Fessard, D., Andres, K.H., Bates, J.A.V., Besson, J.M., Brown, A.G., Burgess, P.R., Darian-Smith, I., v. Düring, M., Gordon, G., Hensel, H., Jones, E., Libet, B., Oscarsson, O., Perl, E.R., Pompeiano, O., Powell, T.P.S., Réthelyi, M., Schmidt, R.F., Semmes, J., Skoglund, S., Szentágothai, J., Towe, A.L., Wall, P.D., Werner, G., Whitsel, B.L., Zotterman, Y., Iggo, A. (Eds.), Somatosensory System, Handbook of Sensory Physiology. Springer, Berlin, Heidelberg, pp. 29–78. https://doi.org/10.1007/978-3-642-65438-1_3

Buzsáki, G., Anastassiou, C.A., Koch, C., 2012. The origin of extracellular fields and currents--EEG, ECoG, LFP and spikes. Nat. Rev. Neurosci. 13, 407–420. https://doi.org/10.1038/nrn3241

Cui, Y., Liu, L.D., McFarland, J.M., Pack, C.C., Butts, D.A., 2016. Inferring Cortical Variability from Local Field Potentials. J. Neurosci. Off. J. Soc. Neurosci. 36, 4121–4135. https://doi.org/10.1523/JNEUROSCI.2502-15.2016

Denker, M., Roux, S., Lindén, H., Diesmann, M., Riehle, A., Grün, S., 2011. The local field potential reflects surplus spike synchrony. Cereb. Cortex N. Y. N 1991 21, 2681–2695. https://doi.org/10.1093/cercor/bhr040

Einevoll, G.T., Kayser, C., Logothetis, N.K., Panzeri, S., 2013. Modelling and analysis of local field potentials for studying the function of cortical circuits. Nat. Rev. Neurosci. 14, 770–785. https://doi.org/10.1038/nrn3599

Flores Ramos, J.M., Devoize, L., Descheemaeker, A., Molat, J.-L., Luccarini, P., Dallel, R., 2017. The nitric oxide donor, isosorbide dinitrate, induces a cephalic cutaneous hypersensitivity, associated with sensitization of the medullary dorsal horn. Neuroscience 344, 157–166. https://doi.org/10.1016/j.neuroscience.2016.12.028

Galindo-Leon, E.E., Liu, R.C., 2010. Predicting stimulus-locked single unit spiking from cortical local field potentials. J. Comput. Neurosci. 29, 581–597. https://doi.org/10.1007/s10827-010-0221-z

Gasser, H.S., Erlanger, J., 1927. The rôle played by the sizes of the constituent fibers of a nerve trunk in determining the form of its action potential wave. Am. J. Physiol.-Leg. Content 80, 522–547. https://doi.org/10.1152/ajplegacy.1927.80.3.522

Geng, X., Wang, X., He, F., Zhang, X., Xie, J., Gao, G., Han, H., Yao, X., Zhang, H., Gao, Y., Wang, Y., Wang, M., 2019. Spike and Local Field Synchronization Between the Pedunculopontine Nucleus and Primary Motor Cortex in a Rat Model of Parkinson's Disease. Neuroscience 404, 470–483. https://doi.org/10.1016/j.neuroscience.2019.01.044

Georgopoulos, A.P., Schwartz, A.B., Kettner, R.E., 1986. Neuronal population coding of movement direction. Science 233, 1416–1419. https://doi.org/10.1126/science.3749885

Hall, T.M., Nazarpour, K., Jackson, A., 2014. Real-time estimation and biofeedback of single-neuron firing rates using local field potentials. Nat. Commun. 5, 5462. https://doi.org/10.1038/ncomms6462

Herreras, O., 2016. Local Field Potentials: Myths and Misunderstandings. Front. Neural Circuits 10, 101. https://doi.org/10.3389/fncir.2016.00101

Kelly, R.C., Smith, M.A., Kass, R.E., Lee, T.S., 2010. Local field potentials indicate network state and account for neuronal response variability. J. Comput. Neurosci. 29, 567–579. https://doi.org/10.1007/s10827-009-0208-9

Lagarias, J.C., Reeds, J.A., Wright, M.H., Wright, P.E., 1998. Convergence Properties of the Nelder--Mead Simplex Method in Low Dimensions. SIAM J. Optim. 9, 112–147. https://doi.org/10.1137/S1052623496303470

Lilliefors, H.W., 1967. On the Kolmogorov-Smirnov Test for Normality with Mean and Variance Unknown. J. Am. Stat. Assoc. 62, 399–402. https://doi.org/10.2307/2283970

Lindén, H., Tetzlaff, T., Potjans, T.C., Pettersen, K.H., Grün, S., Diesmann, M., Einevoll, G.T., 2011. Modeling the spatial reach of the LFP. Neuron 72, 859–872. https://doi.org/10.1016/j.neuron.2011.11.006

Liu, X., Zhou, L., Ding, F., Wang, Y., Yan, J., 2015. Local field potentials are local events in the mouse auditory cortex. Eur. J. Neurosci. 42, 2289–2297. https://doi.org/10.1111/ejn.13003

Maling, N., McIntyre, C., 2016. Chapter 5 - Local Field Potential Analysis for Closed-Loop Neuromodulation, in: El Hady, A. (Ed.), Closed Loop Neuroscience. Academic Press, San Diego, pp. 67–80. https://doi.org/10.1016/B978-0-12-802452-2.00005-6

Melin, C., Jacquot, F., Vitello, N., Dallel, R., Artola, A., 2017. Different processing of meningeal and cutaneous pain information in the spinal trigeminal nucleus caudalis. Cephalalgia Int. J. Headache 37, 1189–1201. https://doi.org/10.1177/0333102416673204

Nauhaus, I., Busse, L., Carandini, M., Ringach, D.L., 2009. Stimulus contrast modulates functional connectivity in visual cortex. Nat. Neurosci. 12, 70–76. https://doi.org/10.1038/nn.2232

Nawrot, M., Aertsen, A., Rotter, S., 1999. Single-trial estimation of neuronal firing rates: From single-neuron spike trains to population activity. J. Neurosci. Methods 94, 81–92. https://doi.org/10.1016/S0165-0270(99)00127-2

Pardalos, P., Principe, J.C. (Eds.), 2002. Biocomputing, Biocomputing. Springer US. https://doi.org/10.1007/978-1-4613-0259-9

Rasch, M.J., Gretton, A., Murayama, Y., Maass, W., Logothetis, N.K., 2008. Inferring spike trains from local field potentials. J. Neurophysiol. 99, 1461–1476. https://doi.org/10.1152/jn.00919.2007

Ray, S., 2015. Challenges in the quantification and interpretation of spike-LFP relationships. Curr. Opin. Neurobiol. 31, 111–118. https://doi.org/10.1016/j.conb.2014.09.004

Ray, S., Maunsell, J.H.R., 2011. Network rhythms influence the relationship between spike-triggered local field potential and functional connectivity. J. Neurosci. Off. J. Soc. Neurosci. 31, 12674–12682. https://doi.org/10.1523/JNEUROSCI.1856-11.2011

Savitzky, Abraham., Golay, M.J.E., 1964. Smoothing and Differentiation of Data by Simplified Least Squares Procedures. Anal. Chem. 36, 1627–1639. https://doi.org/10.1021/ac60214a047

Shimazaki, H., Shinomoto, S., 2010. Kernel bandwidth optimization in spike rate estimation. J. Comput. Neurosci. 29, 171–182. https://doi.org/10.1007/s10827-009-0180-4

Storchi, R., Zippo, A.G., Caramenti, G.C., Valente, M., Biella, G.E.M., 2012. Predicting spike occurrence and neuronal responsiveness from LFPs in primary somatosensory cortex. PloS One 7, e35850. https://doi.org/10.1371/journal.pone.0035850

Vinck, M., Battaglia, F.P., Womelsdorf, T., Pennartz, C., 2012. Improved measures of phase-coupling between spikes and the Local Field Potential. J. Comput. Neurosci. 33, 53–75. https://doi.org/10.1007/s10827-011-0374-4

von Plato, J., 1991. Boltzmann's ergodic hypothesis. Arch. Hist. Exact Sci. 42, 71–89. https://doi.org/10.1007/BF00384333

Zanos, T.P., Mineault, P.J., Pack, C.C., 2011. Removal of spurious correlations between spikes and local field potentials. J. Neurophysiol. 105, 474–486. https://doi.org/10.1152/jn.00642.2010

Zippo, A.G., Nencini, S., Caramenti, G.C., Valente, M., Storchi, R., Biella, G.E.M., 2014. A simple stimulatory device for evoking point-like tactile stimuli: a searchlight for LFP to spike transitions. J. Vis. Exp. JoVE. https://doi.org/10.3791/50941

Model-based signal processing enables bidirectional inferring between local field potential and spikes evoked by noxious stimulation

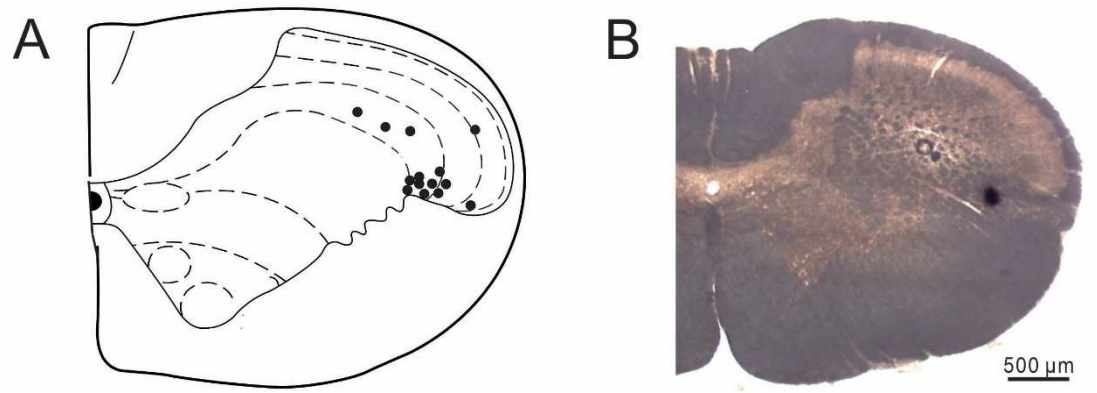

Figure 1. Histologically confirmed and reconstructed loci of single neurons within the medullary dorsal horn. (A) Locations of medullary dorsal horn neurons are summarized on one representative coronal brainstem plane (Interaural -7mm).(B) Microphotograph showing the histologically confirmed recording locus of one trigeminal neuron within the MDH.

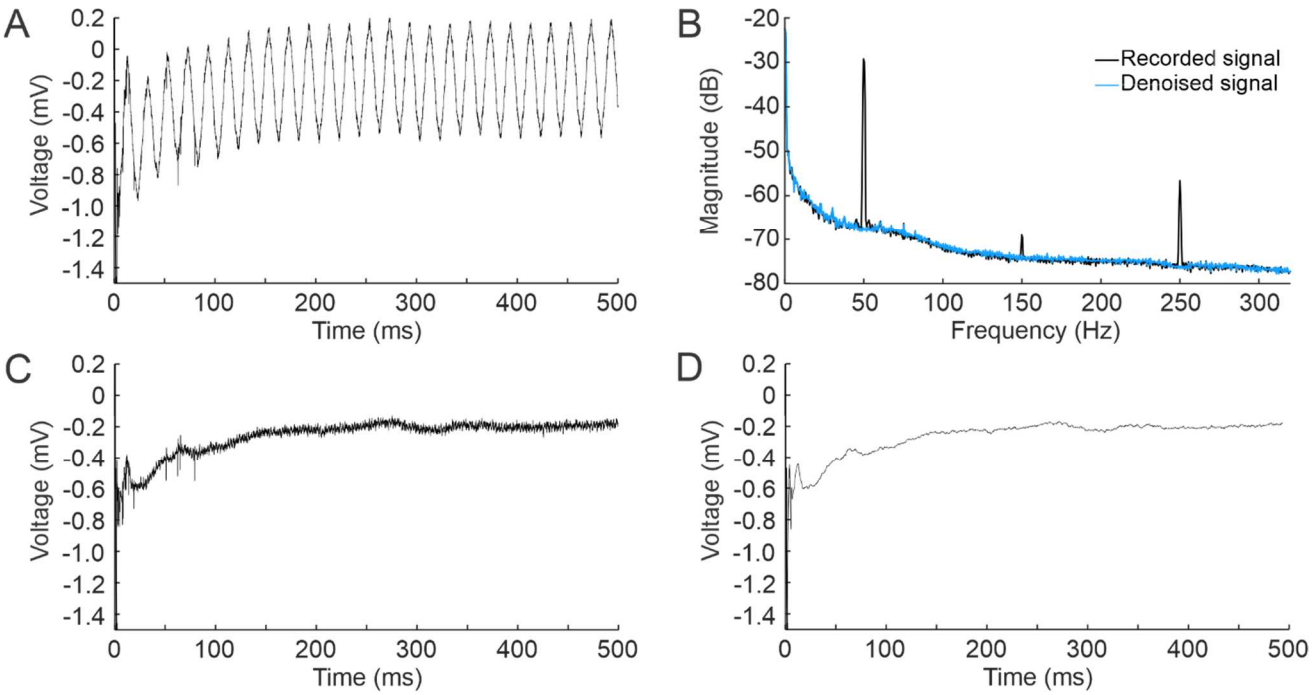

Figure 2. (A) Raw original recording of evoked answer of a MDH neuron, with heavy powerline noise. Voltage in mV against time in ms. (B) Frequency spectrum of original signal and noise free signal (Magnitude in dB vs Frequency in Hz). (C) Same recording as (A), but free from powerline noise. (D) Noise free and spike free evoked answer. Voltage in mV against time in ms.

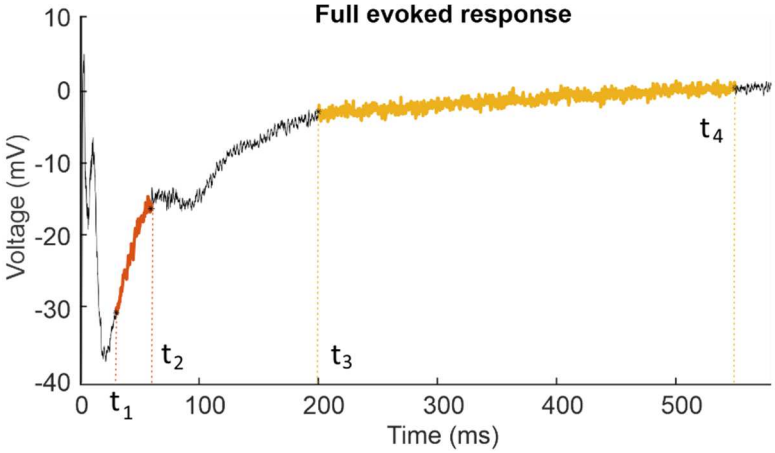

Figure 3. Example of extraction of C-fiber evoked activity in LFP with the full evoked response with portion t_1-t_2 highlighted in red and portion t_3-t_4 highlighted in yellow, amplitude in mV, time in ms

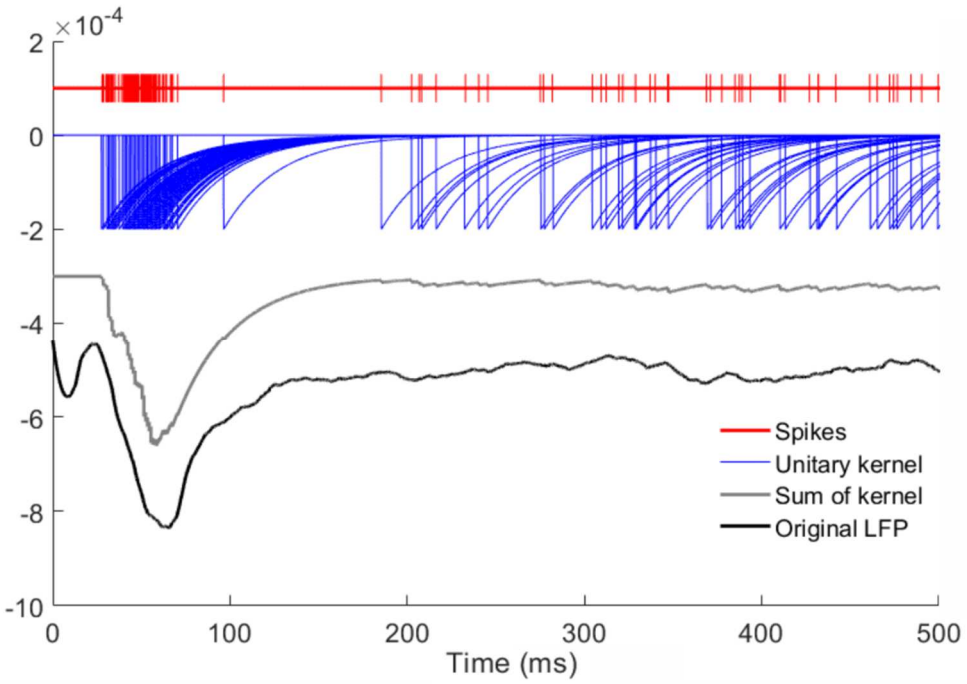

Figure 4. Illustration of the convolution process. Arbitrary amplitude on all the following lines : C-fibers spike timing, convolution kernel as a single decaying exponential (kernel 1), result of the convolution (before smoothing) and C-fiber evoked activity in LFP, against time (in ms).

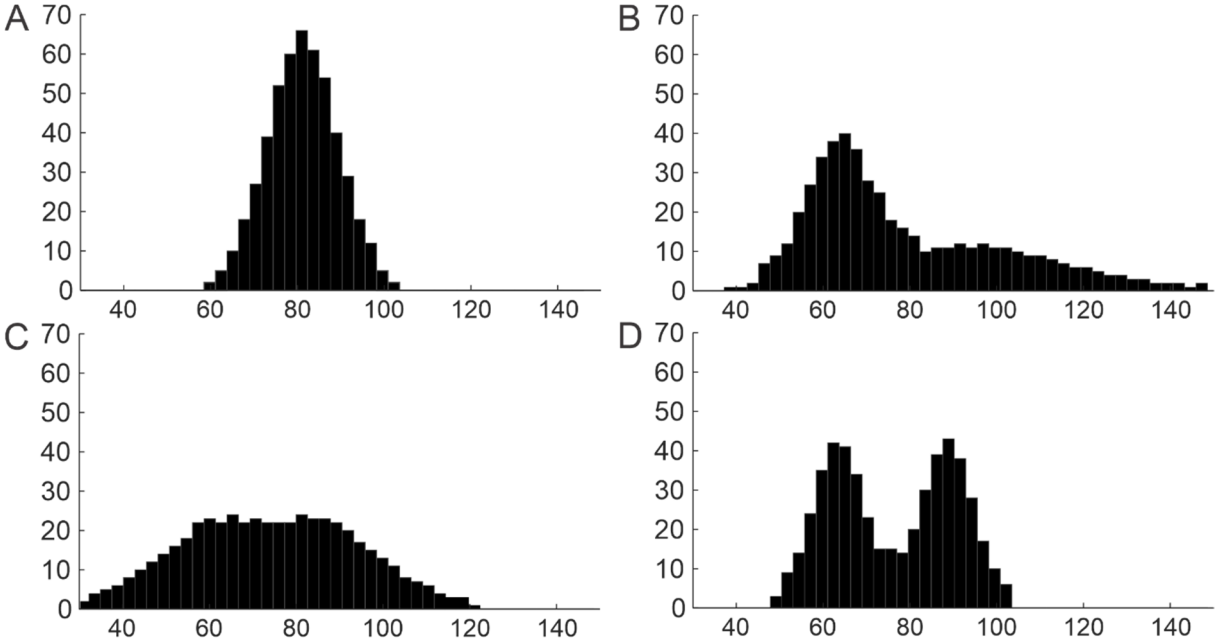

Figure 5. Examples of PSTH calculated from probability density function (distribution 2) with 4 different sets of parameters (N_1, N_2, t_1, t_2, W_1, W_2), chosen to illustrate the ability to produce (A) a PSTH with a single peak shape (250,250,80,85,5,5), (B) an early peak with a late spread (250,250,65,85,5,15), (C) a plateau shape (250,250,67,89,9,9), or (D) a double peak (250,250,65,97,4,4)

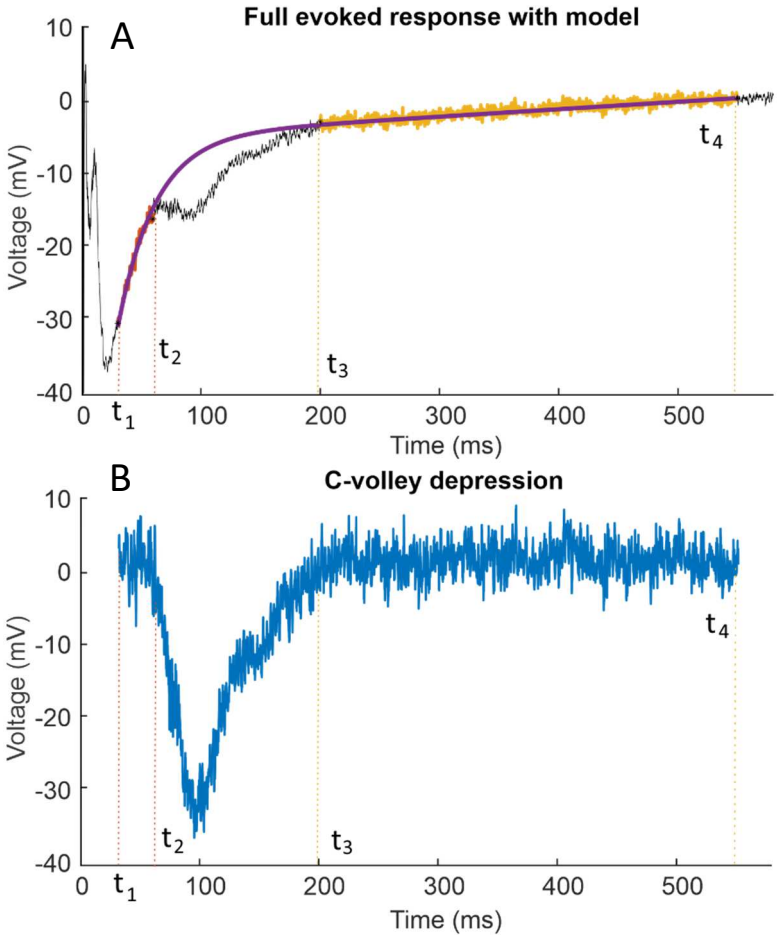

Figure 6. Example of extraction of C-fiber evoked activity in LFP with (A) the full evoked response with the A-fiber LFP model (in purple), amplitude in mV, time in ms; (B) C- fiber LFP only once the model was subtracted from the full response, amplitude in mV, time in ms.

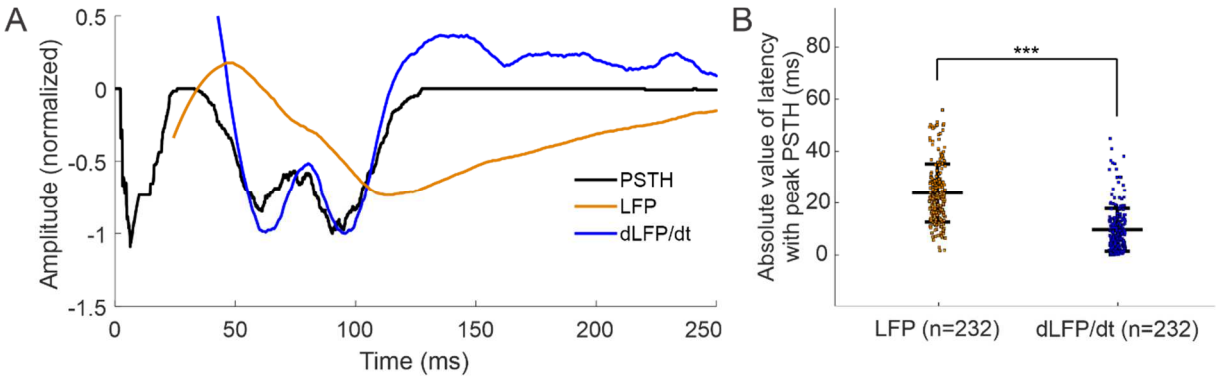

Figure 7. (A) PSTH, LFP and time derivative of LFP for the same set of stimulations. (B) Comparison of absolute latencies between maximum depression of PSTH, and maximum depression of LFP and derivative of LFP (N = 232, paired t-test, $p<10^{-4}$).

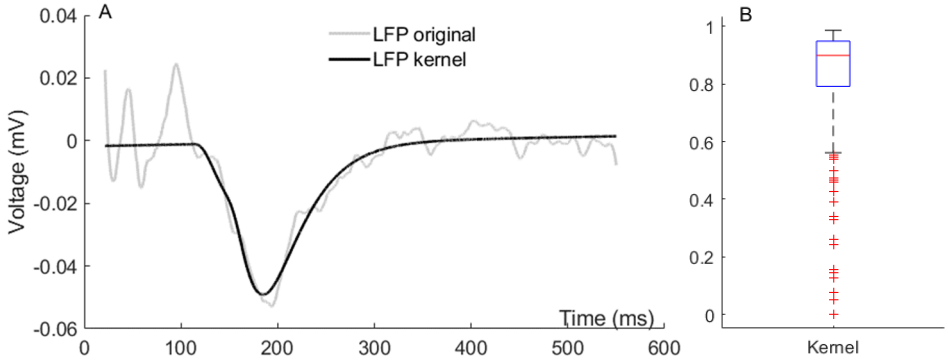

Figure 8. (A) example of goodness-of-fit between measured C-fiber LFP (grey) and calculated C-fiber LFP from the convolution kernel 1 (black). (B) : Pearson correlation coefficients r^2 between measured and calculated C-fiber LFP, for all 232 series

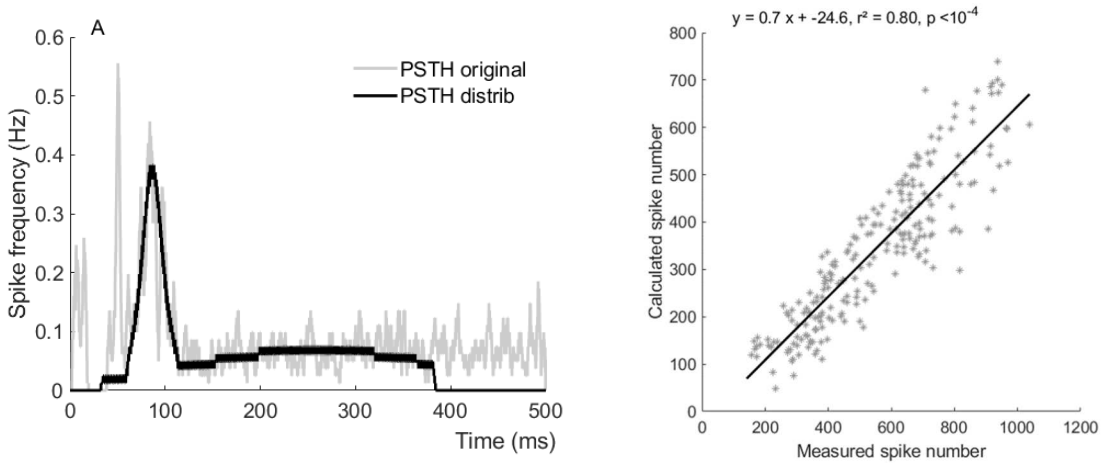

Figure 9. (A) comparison of measured PSTH (grey) and PSTH calculated from kernel and distribution (black). (B) Comparison of number of spikes